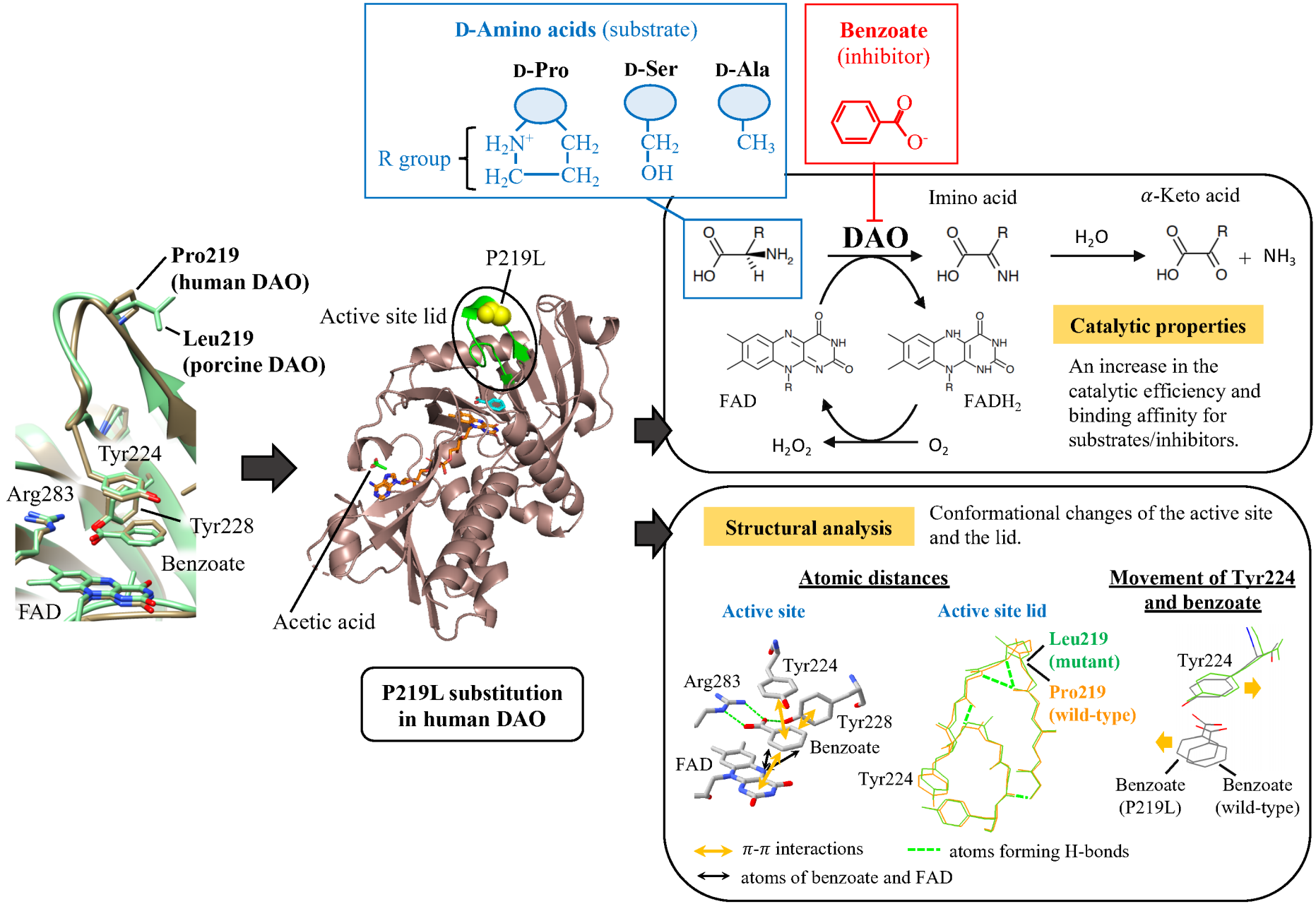

TITLE PAGE

Regular Paper

Title: P219L substitution in human D-amino acid oxidase impacts the ligand binding and catalytic efficiency

Wanitcha Rachadech[1,2], Yusuke Kato[1], Rabab M. Abou El-Magd[1,†], Yuji Shishido[1], Soo Hyeon Kim[1], Hirofumi Sogabe[1], Nobuo Maita[3], Kazuko Yorita[1], Kiyoshi Fukui[1,*]

[1] Division of Enzyme Pathophysiology, Institute for Enzyme Research, Tokushima University, 3-18-15 Kuramoto, Tokushima 770-8503, Japan

[2] Division of Chemistry, Faculty of Science, Udon Thani Rajabhat University, 64 Thahan Road, Muang, Udon Thani, 41000, Thailand

[3] Division of Disease Proteomics, Institute for Enzyme Research, Tokushima University, 3-18-15 Kuramoto, Tokushima 770-8503, Japan

† Present address: Rabab M. Abou El-Magd, Department of Psychiatry, Faculty of Medicine, University of Alberta, Canada

Running title: P219L DAO alters ligand binding and catalytic efficiency

*Kiyoshi Fukui, Division of Enzyme Pathophysiology, Institute for Enzyme Research, Tokushima University, 3-18-15 Kuramoto, Tokushima 770-8503, Japan. Tel: +81-88-633-7430, Fax: +81-88-633-7431, E-mail: kiyo.fukui@tokushima-u.ac.jp

Abbreviations: DAO, D-amino acid oxidase; wild-type, wild-type human DAO; FAD, flavin adenine dinucleotide; H_2O_2, hydrogen peroxide; IPTG, isopropyl ß-D-1-thiogalactopyranoside; PEG4000, polyethylene glycol 4000; SDS, sodium dodecyl sulfate; k_{cat}, catalytic constant; K_m, Michaelis constant; K_i, inhibition constant; K_d, dissociation constant; RMSD, Root Mean Square Deviation; H-bond, Hydrogen bond.

Abstract (200 words)

Human D-amino acid oxidase (DAO) is a flavoenzyme that is implicated in neurodegenerative diseases. We investigated the impact of replacement of proline with leucine at position 219 (P219L) in the active site lid of human DAO on the structural and enzymatic properties, because porcine DAO contains leucine at the corresponding position. The turnover numbers (k_{cat}) of P219L were unchanged, but its K_m values decreased compared to wild-type, leading to an increase in the catalytic efficiency (k_{cat}/K_m). Moreover, benzoate inhibits P219L with lower K_i value (0.7-0.9 μM) compared to wild-type (1.2-2.0 μM). Crystal structure of P219L in complex with flavin adenine dinucleotide (FAD) and benzoate at 2.25 Å resolution displayed conformational changes of the active site and lid. The distances between the H-bond-forming atoms of arginine 283 and benzoate and the relative position between the aromatic rings of tyrosine 224 and benzoate were changed in the P219L complex. Taken together, the P219L substitution leads to an increase in the catalytic efficiency and binding affinity for substrates/inhibitors due to these structural changes. Furthermore, an acetic acid was located near the adenine ring of FAD in the P219L complex. The present study provides new insights into the structure-function relationship of human DAO.

Keywords: human D-amino acid oxidase, point-mutation, active site lid, structure-function relationship, X-ray crystallography

D-amino acid oxidase (DAO, EC 1.4.3.3) is a flavoenzyme that catalyzes the dehydrogenation of D-amino acids to corresponding imino acids with concomitant reduction of flavin adenine dinucleotide (FAD) to reduced form ($FADH_2$). At the active site of DAO, $FADH_2$ is subsequently reoxidized by oxygen to generate hydrogen peroxide (H_2O_2), and the imino acid is spontaneously hydrolyzed to its respective α-keto acid and ammonia (Fig. S1) (*1*). In mammals, DAO is predominantly present in the kidney (*2*), liver (*3*) and brain (*4, 5*). We revealed the cDNA sequences encoding DAOs found in the kidneys of pigs (*6*) and humans (*7*), and discovered a single mRNA species of DAO in the porcine brain (*3*). In addition, the expression of the DAO gene is detected in type-1 astrocytes of the rat cerebellum and cerebral cortex (*8*). The DAO expressed in astrocytes is involved in the metabolism of extracellular D-serine (*9*). Recently, we detected the DAO activity and expression in the epididymis of mice, with the highest level in the caput region (*10*).

Among D-amino acids, D-serine (D-Ser), D-alanine (D-Ala), D-proline (D-Pro), and D-leucine (D-Leu) are present in the brain (*11*). D-Ser has been proposed to serve as the physiological substrate for human DAO (*9*), and to play a role as a neurotransmitter of the *N*-methyl-D-aspartate receptor (NMDAR) (*12*). Therefore, dysfunction of NMDAR may be related to the alteration of the D-Ser level, which is regulated by DAO activity. G72 protein is an important factor to regulate the DAO function (*13*). Hypofunction of NMDAR may play a key role in the pathophysiology of schizophrenia (*14*). In contrast, hyperfunction of NMDAR can lead to excitotoxicity, which is implicated in neurodegenerative disorders, including Alzheimer's disease (*15*) and amyotrophic lateral sclerosis (ALS) (*16*). It has been reported that the substitutions in DAO, including R199W and W209R are involved in ALS, while those including D31H and R279A are involved in schizophrenia (*17-19*).

In 2006, we firstly reported the three-dimensional structure of wild-type human DAO in complex with FAD and the competitive inhibitor benzoate at the resolution of 2.5 Å (PDB ID: 2DU8) (*20*). In the last two decades, thirty-five three-dimensional structures of DAO have been

reported. More than a half of these structures are human DAO. Based on our previous study, human DAO is a homodimer, in which two monomers interact with each other in a head-to-head mode. Each human DAO monomer (347 amino acids, 39 kDa) contains a non-covalently bound FAD cofactor. Moreover, both holo and apo forms of human DAO are stable as homodimers (*21*). A distinctive feature of human DAO is its lower affinity for FAD in comparison to porcine DAO (*20*). The active sites of human and porcine DAOs are covered by a loop composed of residues 216-228, termed the active site lid. It has been proposed that the flexibility of this loop influences the substrate binding and product release in DAO, because the lid is presumed to function as a gate for the entrance and exit of substrates (*22*).

The structure-function relationship of human DAO shed light on the crucial regulatory mechanism of D-Ser metabolism in the human brain, leading to the development of potential modulators of DAO for clinical applications. In line with this, the effects of amino acid substitutions have been assessed to elucidate the mechanism of the DAO catalysis. In comparison to the wild-type, the reduction rates of the Y224F and Y228F mutants of porcine DAO were decreased (*23*). The ability of the Y224F and Y224A mutants of human DAO to bind benzoate was also decreased (*24*). The access of solvent into the active site of DAO through the active site lid is facilitated by introducing Y55A substitution, which may affect the substrate specificity of the enzyme (*25*). Moreover, the substitution of R216-G220 of human D-aspartate oxidase for the active site lid of porcine DAO (I215-N225) has influenced the substrate specificity of DAO (*26*).

Although the genes encoding mammalian DAOs have been cloned, only DAOs from pig and human have been efficiently expressed in the heterologous system such as *E. coli* and well characterized. The kinetic parameters (K_m, k_{cat}, and K_i for benzoate) of human DAO (*20*, *21*) seem to be similar to porcine DAO (*26*, *27*). The K_d values of the binding between DAO and FAD, which were estimated by analyzing the quenching of protein fluorescence, were reported to be different between human and porcine DAOs (human DAO; 8 μM, porcine DAO; 0.2 μM) (*21*). However, the apparent dissociation constant for FAD, which was determined by measuring

the FAD-dependent activity of human DAO, was 0.2 μM (*28*). Even though the characteristics of human DAO have been well described previously, the functional role of Pro at the position 219, which is conserved in most mammalian DAOs except the porcine DAO, has not been investigated. Therefore, Pro219 to Leu substitution (P219L) was introduced to human DAO, because porcine DAO has Leu at the corresponding position (*29*). In the present study, the kinetic parameters and crystal structure of P219L human DAO were analyzed and compared to wild-type human DAO to elucidate the catalytic role of the Pro219 residue.

Materials and Methods

Chemical reagents

D-Pro, D-Ala, D-Ser, FAD, potassium bromide (KBr), potassium chloride (KCl), sodium dodecyl sulfate (SDS), phenylmethylsulfonyl fluoride (PMSF), ampicillin, glycerol, isopropyl ß-D-1-thiogalactopyranoside (IPTG), polyethylene glycol (PEG) 4000, ammonium acetate, and sodium citrate were purchased from Wako Pure Chemical Industries (Osaka, Japan). Yeast extract, tryptone, sodium chloride (NaCl), glucose and ammonium sulfate were obtained from Nacalai Tesque (Kyoto, Japan). Lysozyme and sodium benzoate were purchased from Sigma-Aldrich (St Louis, MO, USA).

Bacterial cultivation and enzyme production

E. coli cells BL21 (DE3) harboring pET11b/wild-type human DAO and pET11b/P219L human DAO plasmids, which were established in previous reports (*20*, *29*) were streaked on a Luria-Bertani (LB) agar plate (1% tryptone, 0.5% yeast extract, and 1% NaCl, w/v) containing 50 µg. mL^{-1} ampicillin and incubated at 37°C for 16 h. A single colony was inoculated into 5 mL LB broth media containing 50 µg. mL^{-1} ampicillin and incubated at 37°C for 16 h with shaking at 125 rpm. One milliliter of starter culture (1% (v/v)) was inoculated into 100 mL of LB media in a 500 mL flask containing 50 µg. mL^{-1} ampicillin and incubated at 37°C for 16 h with shaking at 125 rpm. Twenty milliliters of starter culture (2% (v/v)) was inoculated into 1 L of fresh Terrific broth (1.2% (w/v) tryptone, 2.4% (w/v) yeast extract and 0.4% (v/v) glycerol in potassium phosphate buffer) containing 50 µg. mL^{-1} ampicillin, 0.5% (w/v) glucose and 250 µL of antifoam B in a 2 L flask. Incubation at 37°C with 170 rpm rotary shaking was performed until the OD_{600} reached 1.8-2.0. The expression of DAO was induced by adding 0.1 mM IPTG. The cell culture was further incubated at the same condition for an additional 20 h, and then harvested by centrifugation (Beckman Coulter, J6-MI, Ireland) at 4,500 ×g for 45 min at 4°C. The cell pellets were resuspended in the lysis buffer (17 mM sodium pyrophosphate, pH 8.3 containing 0.3 mM EDTA,

1 mM benzoate, 100 μM FAD, 0.5 mM dithiothreitol and 4.5 μg. mL^{-1} PMSF) and stored at –80°C.

Purification of holo human DAO and the measurement of enzymatic activity

The wild-type and P219L human DAOs in holo form were purified using the modified procedure for recombinant DAO from pig (*30*) and human (*20*). All procedures were conducted at 4°C unless otherwise stated. The frozen cells were thawed and suspended in the lysis buffer. After adding 0.5 mg. mL^{-1} lysozyme to disrupt *E. coli* cells, 1% (w/v) streptomycin sulfate was then added to the cell lysate. The debris was removed by centrifugation. The collected supernatant was heated for 3 min after the temperature reached 53°C, and immediately transferred to the ice box. After centrifugation, 45% (w/v) ammonium sulfate was added to the supernatant and centrifuged to obtain pellets. The pellets were resuspended in buffer A (10 mM Tris-HCl, pH 7.4 containing 125 mM KCl, 0.2 mM benzoate, 40 μM FAD and 4.5 μg. mL^{-1} PMSF), and dialyzed overnight against the same buffer. After centrifugation, the supernatant was applied to the DEAE Sepharose Fast Flow column (Sigma-Aldrich, USA) equilibrated with buffer A. The eluated fractions containing human DAO were detected based on the OD_{280}/OD_{458} ratio using a spectrophotometer (DU600-Beckman, USA), and precipitated with 70% (w/v) ammonium sulfate. After dialysis overnight against buffer B (50 mM sodium phosphate, pH 6.8 containing 0.2 mM benzoate and 40 μM FAD), the supernatant was loaded into the hydroxyapatite column (Nacalai Tesque, Japan), which was equilibrated with buffer B. Again, the eluated fractions containing human DAO were detected and precipitated with 70% (w/v) ammonium sulfate. Finally, the purified human DAO in holo form was obtained. The purity of DAO was confirmed by SDS-PAGE. The concentration of DAO was estimated with a BCA Protein Assay Kit (Pierce, Rockford, IL, USA) using BSA as a standard protein.

The human DAO activity was determined based on the rate of oxygen consumption using an Oxygraph Plus system (Hansatech instruments, UK) in air-saturated solution. The assay was

carried out at 25°C in 100 mM sodium phosphate (pH 8.0), containing 20 μM FAD and 20 mM D-Ala. The enzymatic reaction was started by adding 0.1 μM human DAO. The concentration of holo DAO was determined based on the extinction coefficient at 458 nm (12.3 mM^{-1} cm^{-1}). One unit of DAO activity was defined as the amount of enzyme that consumes 1 micromole of oxygen per min.

Preparation of apo DAO

In order to prepare apo DAO, holo DAO was dialyzed against 50 mM sodium pyrophosphate buffer (pH 8.3) containing 1 M KBr (*31*), 1 mM EDTA, and 1% (w/v) activated charcoal at 4°C until the yellow color of the holoenzyme solution disappeared. To completely remove KBr, the colorless solution containing apo DAO was dialyzed against the same buffer without KBr for one to two days. The concentration of apo DAO was determined based on the extinction coefficient at 280 nm (73 mM^{-1} cm^{-1}) (*32*).

Determination of kinetic parameters for holo and reconstituted DAOs

The procedures to determine the apparent kinetic parameters of holo and reconstituted DAOs were modified from the method used to characterize recombinant human DAO (*20, 28*). The composition of the pre-reaction mixture was 0.3 mM EDTA and 100 mM sodium phosphate (pH 8.0). For the assays of reconstituted DAO, 0.1 μM apo DAO and 2 μM FAD were added to the pre-reaction mixture and incubated for 3 min. Subsequently, various concentrations (up to 10 mM) of D-amino acid were added to start the reaction. The dissociation constant (K_d) of FAD from DAO was investigated by adding various concentrations of FAD. To determine the kinetic parameters of holo DAO, 50 mM sodium pyrophosphate (pH 8.3) was also used instead of sodium phosphate. FAD (20 μM) and various concentrations of D-amino acid were added to the pre-reaction mixture and incubated in the presence (0.1-10 μM) or absence of benzoate before 0.1 μM holo DAO was added to this mixture. The kinetic parameters of enzymatic reactions were

calculated from conventional Michaelis-Menten equation (*27, 33*). The turnover number (k_{cat}) is expressed as micromoles of oxygen consumed per min per micromole of DAO.

X-ray crystallography and structure determination

P219L DAO in the holo form mixed with 40 μM FAD and 0.2 mM benzoate was concentrated up to 12 mg. mL^{-1} using Centriprep (30 kDa cutoff, Merck Millipore, Germany). The screening of crystallization conditions was conducted by the hanging-drop vapor diffusion method. X-ray diffraction data were collected on beamline BL5A at Photon Factory. Scaling, molecular replacement and model building were performed with iMosfilm (*34*), XDS (*35*), MolRep (*36*) and Coot (*37*). Crystallographic refinement was carried out as previously described using Phenix (*38, 39*). The Ramachandran plot of the final structure was validated by RAMPAGE (*40*). RMSD values were calculated with Swiss-PdbViewer (*41*).

Results

Preparation of wild-type and P219L DAOs

The amino acid sequence alignment showed that human DAO possesses Pro219, which is conserved in most mammalian DAOs (Fig. S2, A). However, porcine DAO possesses Leu at the corresponding position, which is located at the tip of the active site lid (Fig. S2, B). The conformation of the active site lid in human DAO was also different from porcine DAO (Fig. S2, B). To analyze the impact of the 219th residue on the activity and structure of human DAO, we produced wild-type and P219L mutant of human DAO. Both wild-type and P219L were expressed in *E. coli* cells under the same conditions. The cell walls were broken by lysozyme. The partial purification procedures were carried out by heat treatment at 53°C, in which the majority of holo human DAO molecules in complex with benzoate should be stable (*42*), followed by 45% (w/v) ammonium sulfate precipitation. The estimated yields of wild-type and P219L were 4 and 1.8 mg purified proteins per 1 L of culture after the final column chromatography with hydroxyapatite, respectively (Table S1). Moreover, the specific activities of purified wild-type and P219L were 10.4 and 9.3 U/mg protein with 52-fold and 46.5-fold degrees of purity in comparison to the cell lysate, respectively. The purities of wild-type and P219L were confirmed by SDS-PAGE stained with Coomassie blue, as shown in Fig. S3, A and B, respectively.

Determination of the kinetic parameters of wild-type and P219L under low and high FAD concentrations

To assess the functional characteristics of purified DAO, we used an oxygen electrode to measure the rate of oxygen consumption in the assay solution. According to our previous findings, human DAO preferably catalyzes uncharged D-amino acids (*i.e.*, D-Ser, D-Ala, and D-Pro) (*43*). In the present work, we found that the k_{cat}, K_m, and k_{cat}/K_m values of wild-type for all tested substrates (D-Ser, D-Ala, and D-Pro) were consistent with our previous study. Since human DAO was reported to show low affinity for FAD (*21*), a high FAD concentration (final conc. ~20 μM FAD

in the assay solution), was applied to reconstitute an active holo DAO and to examine its kinetic characteristics (Fig. 1). The kinetic parameters of wild-type were compared to those of P219L. The k_{cat} values of holo DAOs of both wild-type and P219L in which DAOs were saturated with FAD were similar under high concentrations of FAD (Fig. 1A). In contrast, the K_m values of wild-type were approximately 2-fold greater than those of P219L for three different substrates (Fig. 1B), which suggests that the substrate-binding affinity of wild-type is lower than that of P219L. The k_{cat}/K_m values of wild-type were approximately 2-fold lower than those of P219L (Fig. 1C). Among tested substrates, it is suggested that D-Ala has the strongest binding affinity for both wild-type and P219L based on the smallest K_m values, followed by D-Pro. It is suggested that D-Ser has the weakest binding affinity for human DAO. D-Pro showed the highest catalytic efficiency (k_{cat}/K_m) in the cases of both wild-type and P219L, followed by D-Ala and D-Ser.

The physiological FAD concentrations in various organs in mice are in the range of 2-15 μM (*44*). Thus, the effect of a low FAD concentration (final conc. ~2 μM FAD in the assay solution) was examined to mimic the physiological condition in the kinetic analysis using reconstituted human DAO from apo DAO and FAD. The k_{cat} values of both wild-type and P219L were similar (Fig. 2A). However, P219L showed approximately 2-fold lower K_m values and higher k_{cat}/K_m values in comparison to wild-type for all substrates, as observed in Fig. 2B and 2C, respectively. These values are in good agreement with our previous values of wild-type human DAO in the condition with a low concentration of FAD (*45*). The K_d for FAD was estimated from a Lineweaver-Burk plot in which the initial velocities of the reactions were plotted against the concentrations of FAD. We found that the K_d value of P219L was slightly but significantly different from that of wild-type (P219L; 0.146 ± 0.009 μM, wild-type; 0.173 ± 0.003 μM, $p < 0.01$). The K_d value of wild-type was consistent with our previous study (*28*). The kinetic parameters of reconstituted human DAO in the condition with a low concentration of FAD (Fig. 2) were compared to the parameters of holo-human DAO in the condition with a high concentration of FAD (Fig. 1). The K_m values of FAD-reconstituted human DAO (Fig. 2B)

for all the substrates were greater than those of holo-human DAO (Fig. 1B). However, the k_{cat} and k_{cat}/K_m values of FAD-reconstituted human DAO, as shown in Fig. 2A and 2C, were lower than those of holo-human DAO (Fig. 1A and 1C). Our results with low and high concentrations of FAD indicated that the replacement of Pro at position 219 located in the active site lid of human DAO with Leu alters the substrate-binding affinity (K_m) and catalytic efficiency (k_{cat}/K_m) of the enzyme. In addition, both wild-type and P219L preferred to catalyze hydrophobic substrates (D-Ala and D-Pro) in comparison to the hydrophilic substrate (D-Ser), because the hydrophobic substrates showed higher k_{cat}/K_m and lower K_m values.

Alteration of the affinity for benzoate with P219L substitution

Subsequently, we determined the inhibition constant (K_i) of the competitive inhibitor benzoate for human DAO. The initial velocities of enzymatic reaction were measured under various benzoate concentrations and fitted to a Lineweaver-Burk plot. We found that the K_i values of benzoate for wild-type were in the range of 1.2-2.0 μM with three different substrates, including D-Pro, D-Ala and D-Ser, while the values for P219L were in the range of 0.7-0.9 μM. These K_i values for P219L were approximately 2-fold lower than those for wild-type (Fig. 3). In other words, P219L showed tighter binding to the inhibitor benzoate than wild-type. The observed K_i values for P219L with the substrates D-Pro and D-Ser were significantly lower than those for wild-type. These results indicated that the P219L substitution altered the inhibition constant (K_i) of benzoate.

Structure determination of P219L in complex with FAD and benzoate

In order to provide a structural basis for the difference in the kinetic parameters between wild-type and P219L, we determined the crystal structure of the ternary complex of P219L, FAD and benzoate at 2.25 Å resolution. The statistics for data collection and refinement are summarized in Tables I and II. The overall structure of the P219L complex was quite similar to that of the

wild-type complex (PDB ID: 2DU8) (*20*) with a backbone RMSD value of ~0.4 Å. We found that the B-factor of benzoate of the P219L complex (39.30 Å^2) (Table II) was lower than that of the wild-type complex (60.29 Å^2) (*20*) whereas the B-factors of the other regions showed comparable values between these ternary complexes. These results indicated that the mobility of benzoate in the wild-type complex may be different from that in the P219L complex. The conformation of the hydrophobic stretch (residues 47-51, VAAGL) in P219L was virtually identical to that in wild-type with a backbone RMSD value of ~0.2 Å. The distance between the isoalloxazine ring N5 atom and the Ala49 backbone N atom in P219L was similar to that in wild-type (P219L; 3.91 ± 0.08 Å, wild-type; 3.78 ± 0.08 Å). These results suggested that the P219L substitution did not affect the conformation of the hydrophobic stretch in human DAO.

Structure of the active site and the active site lid

A negative charge at benzoate was neutralized by Arg283 of P219L, which also formed H-bonds with benzoate together with Tyr228 (Fig. 4A). The aromatic ring of benzoate was sandwiched between the isoalloxazine ring of FAD and the side chain ring of Tyr224. These characteristics are in excellent agreement with the wild-type structure (*20*). The distances between the carboxylate group of benzoate and H-bond donors in Tyr228 and Arg283 of P219L were shorter than those in the wild-type complex, suggesting stronger binding in the P219L complex ((1) - (3) in Fig. 4A). The benzoate-FAD distance in the wild-type complex was slightly different from that in the P219L complex ((4), (5) in Fig. 4A). Thus, the relative position of benzoate with respect to FAD differed between the wild-type and P219L complexes. These results are consistent with the results of the kinetic analysis of human DAO inhibition, as shown in Fig. 3, in which the K_i value of benzoate for P219L was approximately 2-fold lower than that for wild-type, suggesting stronger binding of P219L with benzoate.

The conformation of the active site lid of P219L was slightly different from wild-type (Fig. 4B) with a backbone RMSD of 0.54 Å. We further compared distances between the H-bond-

forming atoms in the active site lid, and found that the H-bond distances of Asp218 (C=O) - Arg221 (NH) and Asp218 (C=O) - Gly222 (NH) of P219L were altered in comparison to wild-type (Fig. 4B). However, the H-bond distances of Gly222 (C=O) - Asn225 (NH) and Pro227 (C=O) - Thr216 (NH) of P219L were similar to wild-type. In addition, the B-factor of amino acid residues in the active site lid in P219L (49.65 $Å^2$) was lower than that in wild-type (57.95 $Å^2$) (Table S2). In particular, the B-factor of Tyr224 in P219L was 41.76 $Å^2$, whereas that in wild-type was 58.72 $Å^2$. These results suggested that the P219L substitution affects the conformation and flexibility of the active site lid for substrate entry and product release.

The structural change of Tyr224 and benzoate in the P219L complex

The aromatic ring of Tyr224 plays an important role as the gate to sequester the active site of human DAO from solvent (*46*). In comparison to the wild-type complex, the relative location of the aromatic ring of benzoate with respect to that of Tyr224 in the P219L complex was shifted (Fig. 5). This movement may influence the extent of the π-π interaction between these aromatic rings. These results indicated that the P219L substitution could alter the binding affinity between Tyr224 and ligands, including substrates and inhibitors.

Acetic acid in the ternary complex of P219L

We found a pronounced blob at one of the entrance/exit pathways of the cavity that accommodates FAD in the electron density map of individual P219L molecules within the asymmetric unit (Fig. 6A). The blob was close to the pocket that accommodates the adenine ring of FAD, the adenine ring pocket. The shapes of the blobs were identical to that of the acetic acid molecule, which was one of the compounds used to prepare the crystal (Fig. S4). Thus, the blobs in molecule B (Fig. S4) and D within the asymmetric unit were identified as acetic acid. A water molecule located closely to the acetic acid molecule bridged the acetic acid, adenine ring and neighboring residues, including Lys163 and Trp185, through H-bonds (Fig. 6B). The amino

acid residues surrounding the acetic acid molecule were negative (*i.e.*, Asp37, Glu165, and Glu249), positive (*i.e.*, Arg38, and Lys163), aromatic (*i.e.*, Trp185), and other residues (*i.e.*, Thr43, and Ala188) (Fig. 6B).

Accession code

The structure factors of the P219L and its atomic coordinates have been deposited in the Protein Data Bank with accession code 6KBP.

Discussion

In the present study, we investigated the impact of the replacement of Pro219 at the active site lid with Leu on the structure and function of human DAO, because porcine DAO has Leu at the corresponding position. We found differences in the kinetic parameters (*i.e.*, K_m, k_{cat}/K_m and K_i values) between P219L and wild-type DAOs in conditions with high and low concentrations of FAD. In addition, the structures of the active site and the lid of the P219L complex were different from those of the wild-type complex. We also found an acetic acid molecule that was located close to the adenine ring of FAD in the P219L complex.

The K_m values of P219L were lower than those of wild-type (Fig. 1B and 2B). In other words, P219L has stronger substrate-binding affinity than wild-type. Among tested D-amino acids, D-Ala showed the smallest K_m value for both P219L and wild-type, which suggests the strongest binding affinity of D-Ala to DAO. The side chain of D-Ala has stronger hydrophobicity than the other D-amino acids used in the present study (*i.e.*, D-Pro and D-Ser) (*47*). A substrate side chain in the substrate-binding pocket of DAO extends toward the secondary pocket, which is formed by an array of several hydrophobic residues (*39, 43, 48*). Thus, the hydrophobic side chains of substrates are stabilized in the secondary pocket through hydrophobic interactions. The k_{cat} values were similar between P219L and wild-type in both the high (final conc. ~20 μM, Fig. 1) and low (final conc. ~2 μM, Fig. 2) FAD concentrations (Fig. 1A and 2A). The rate-limiting step of human DAO catalysis has been defined as that of product release (*21*), which suggests that the P219L substitution did not impact the rate of oxygen consumption of the enzyme. These findings suggested that the conformation of the active site or/and the active site lid in P219L was not associated with the product dissociation rate of the enzyme.

We investigated the impact of a change in the FAD concentration on the characteristics of human DAO. The condition with a low concentration of FAD mimicked the physiological FAD concentration, whereas DAO was saturated with FAD in the condition with a high concentration

of FAD. K_m values of FAD-reconstituted human DAO with a low concentration of FAD were greater than those of holo-human DAO in the condition with a high concentration of FAD, while k_{cat} and k_{cat}/K_m values were lower (Fig. 2). Interestingly, the profiling patterns of the individual kinetic parameters depending on substrate species were quite similar between the conditions with low and high concentrations of FAD, although the magnitude of these parameters differed between the conditions (Fig. 1, 2). Our previous study reported that human DAO weakly interacts with FAD (*21*). The conformation of the hydrophobic stretch (residues 47-51, VAAGL) in human DAO was suggested to play a key role in the binding affinity for FAD (*20*). In the present study, the conformation of the hydrophobic stretch in P219L was virtually identical to that in wild-type. The K_d for binding of FAD to P219L was slightly different from that to wild-type. In addition, both holo- and apo-human DAOs, which are in equilibrium under physiological conditions, are stable as a homodimer (*21*). Thus, we hypothesize that the kinetic analysis under the low concentration of FAD reflects the dynamic regulation of DAO activity in the equilibrium between holo- and apo- human DAO under the physiological condition.

It has been reported that the hydroxy group of Tyr228 and guanidino group of Arg283 play important roles in the binding between DAO and ligands (*20, 27, 49, 50*). The crystal structure of the ternary complex of P219L, FAD and benzoate revealed that the conformation of the active site lid was altered in comparison to wild-type (Fig. 4B). The distances between the H-bond-forming atoms of Arg283, Tyr228 and benzoate (Fig. 4A), as well as the relative position between the aromatic rings of Tyr224 and benzoate (Fig. 5), were also altered in the P219L complex. We hypothesize that the replacement of Pro219 with Leu leads to the loop region more flexible because Pro gives the rigidity in the conformation of the mainchain. The flexibility impacts the positional shift of Tyr224. However, it may be difficult to accurately evaluate the conformational changes of the active site lid of P219L compared to wild-type due to the high flexibility of the active site lid.

In addition, the B-factor for benzoate in the P219L complex was different from the wild-type complex (Table II and Fig. 5). These changes in the P219L complex caused a decrease in the inhibition constant (K_i) of benzoate, that is, an increase in the affinity for benzoate, compared with wild-type (Fig. 3) in part through the change in the extent of the π-π interaction between Tyr224 and benzoate aromatic rings. The π-π interaction between two benzene aromatic rings is most stable when the aromatic rings are in the parallel-displaced conformer, as observed in the Tyr224 and benzoate of the DAO complexes (*51*). In the reductive half-reaction of DAO, Tyr224 could stabilize the second charge-transfer intermediate by interacting with the positive charge of imino acid (*23*). Tyr224 residue is involved not only in the interaction with benzoate (*24*) but also plays an important role in the determination of substrate specificity (*22, 26*). Therefore, the relative position between Tyr224 and a substrate/inhibitor is presumed to be an indispensable factor in determining the binding affinity and specificity of human DAO to substrates/inhibitors.

Hallberg *et al*. reported that acetate molecule was bound to the active site of the flavoenzyme pyranose 2-oxidase (*52*). They also confirmed that acetate, originated from the buffer used for crystallization, was a competitive inhibitor of this enzyme. However, the acetate molecule binding to any of DAO structure has not been reported so far. In the P219L complex, an acetic acid molecule was located close to an adenine ring of FAD (Fig. 6). The presence of the acetic acid molecule might impact the binding affinity of FAD, because the acetic acid molecule appears to contribute to stabilizing the conformation of the adenine ring pocket by polar interactions with charged residues around the pocket, as well as H-bonds through a bridging water molecule. The adenine ring was surrounded by the acetic acid molecule and an adenine-binding motif composed of Ile6, Lys163, Val164 and Glu165 (*53*). The aliphatic-aromatic interactions play an important role in packing of adenine ring in the adenine binding pocket of a protein (*54*). In addition to the adenine-surrounding residues, including Ile6 and Val164, the methyl group of the acetic acid molecule may interact with the adenine ring through the

aliphatic-aromatic interaction to stabilize the structure of the adenine-binding pocket. The functional relevance of the acetic acid binding to the enzyme remains to be investigated.

References

1. Krebs, H.A. (1935) Metabolism of amino acids: deamination of amino acids. *Biochem. J.* **29**, 1620–1644
2. Konno, R. and Yasumura, Y. (1983) Mouse mutant deficient in D-amino acid oxidase activity. *Genetics* **103**, 277–285
3. Fukui, K., Momoi, K., Watanabe, F., and Miyake, Y. (1988) In vivo and in vitro expression of porcine D-amino acid oxidase: in vitro system for the synthesis of a functional enzyme. *Biochemistry* **27**, 6693–6697
4. Konno, R. and Yasumura, Y. (1984) Brain and kidney D-amino acid oxidases are coded by a single gene in the mouse. *J. Neurochem*. **42**, 584–586
5. Goldstein, D.B. (1966) D-Amino acid oxidase in brain: distribution in several species and inhibition by pentobarbitone. *J. Neurochem*. **13**, 1011–1016
6. Fukui, K., Watanabe, F., Shibata, T., and Miyake, Y. (1987) Molecular cloning and sequence analysis of cDNAs encoding porcine kidney D-amino acid oxidase. *Biochemistry* **26**, 3612–3618
7. Momoi, K., Fukui, K., Watanabe, F., and Miyake, Y. (1988) Molecular cloning and sequence analysis of cDNA encoding human kidney D-amino acid oxidase. *FEBS Lett*. **238**, 180–184
8. Urai, Y., Jinnouchi, O., Kwak, K.T., Suzue, A., Nagahiro, S., and Fukui, K. (2002) Gene expression of D-amino acid oxidase in cultured rat astrocytes: regional and cell type specific expression. *Neurosci. Lett*. **324**, 101–104

9. Park, H.K., Shishido, Y., Ichise-Shishido, S., Kawazoe, T., Ono, K., Iwana, S., Tomita, Y., Yorita, K., Sakai, T., and Fukui, K. (2006) Potential role for astroglial D-amino acid oxidase in extracellular D-serine metabolism and cytotoxicity. *J. Biochem*. **139**, 295–304
10. Kim, S.H., Shishido, Y., Sogabe, H., Rachadech, W., Yorita, K., Kato, Y., and Fukui, K. (2019) Age- and gender-dependent D-amino acid oxidase activity in mouse brain and peripheral tissues: implication for aging and neurodegeneration. *J. Biochem*. **166**, 187–196
11. Verrall, L., Burnet, P.W.J., Betts, J.F., and Harrison, P.J. (2010) The neurobiology of D-amino acid oxidase and its involvement in schizophrenia. *Mol. Psychiatry* **15**, 122–137
12. Martineau, M., Baux, G., and Mothet, J.P. (2006) D-Serine signalling in the brain: friend and foe. *Trends Neurosci*. **29**, 481–491
13. Chumakov, I., Blumenfeld, M., Guerassimenko, O., Cavarec, L., Palicio, M., Abderrahim, H., Bougueleret, L., Barry, C., Tanaka, H., La Rosa, P., Puech, A., Tahri, N., Cohen-Akenine, A., Delabrosse, S., Lissarrague, S., Picard, F.P., Maurice, K., Essioux, L., Millasseau, P., Grel, P., Debailleul, V., Simon, A.M., Caterina, D., Dufaure, I., Malekzadeh, K., Belova, M., Luan, J.J., Bouillot, M., Sambucy, J.L., Primas, G., Saumier, M., Boubkiri, N., Martin-Saumier, S., Nasroune, M., Peixoto, H., Delaye, A., Pinchot, V., Bastucci, M., Guillou, S., Chevillon, M., Sainz-Fuertes, R., Meguenni, S., Aurich-Costa, J., Cherif, D., Gimalac, A., Van Duijn, C., Gauvreau, D., Ouellette, G., Fortier, I., Raelson, J., Sherbatich, T., Riazanskaia, N., Rogaev, E., Raeymaekers, P., Aerssens, J., Konings, F., Luyten, W., Macciardi, F., Sham, P.C., Straub, R.E., Weinberger, D.R., Cohen, N., and Cohen, D. (2002) Genetic and physiological data implicating the new human gene G72 and the gene for D-amino acid oxidase in schizophrenia. *Proc. Natl. Acad. Sci. U.S.A.* **99**, 13675–13680
14. Almond, S.L., Fradley, R.L., Armstrong, E.J., Heavens, R.B., Rutter, A.R., Newman, R.J., Chiu, C.S., Konno, R., Hutson, P.H., and Brandon, N.J. (2006) Behavioral and

biochemical characterization of a mutant mouse strain lacking D-amino acid oxidase activity and its implications for schizophrenia. *Mol. Cell. Neurosci*. **32**, 324–334

15. Hashimoto, K., Fukushima, T., Shimizu, E., Okada, S.I., Komatsu, N., Okamura, N., Koike, K., Koizumi, H., Kumakiri, C., Imai, K., and Iyo, M. (2004) Possible role of D-serine in the pathophysiology of Alzheimer's disease. *Prog. Neuropsychopharmacol. Biol. Psychiatry* **28**, 385–388
16. Sasabe, J., Chiba, T., Yamada, M., Okamoto, K., Nishimoto, I., Matsuoka, M., and Aiso, S. (2007) D-Serine is a key determinant of glutamate toxicity in amyotrophic lateral sclerosis. *EMBO J*. **26**, 4149–4159
17. Mitchell, J., Paul, P., Chen, H.J., Morris, A., Payling, M., Falchi, M., Habgood, J., Panoutsou, S., Winkler, S., Tisato, V., Hajitou, A., Smith, B., Vance, C., Shaw, C., Mazarakis, N.D., and de Belleroche, J. (2010) Familial amyotrophic lateral sclerosis is associated with a mutation in D-amino acid oxidase. *Proc. Natl. Acad. Sci. U.S.A.* **107**, 7556–7561
18. Caldinelli, L., Sacchi, S., Molla, G., Nardini, M., and Pollegioni, L. (2013) Characterization of human DAAO variants potentially related to an increased risk of schizophrenia. *Biochim. Biophys. Acta* **1832**, 400–410
19. Cappelletti, P., Piubelli, L., Murtas, G., Caldinelli, L., Valentino, M., Molla, G., Pollegioni, L., and Sacchi, S. (2015) Structure-function relationships in human D-amino acid oxidase variants corresponding to known SPNs. *Biochim. Biophys. Acta* **1854**, 1150–1159
20. Kawazoe, T., Tsuge, H., Pilone, M.S., and Fukui, K. (2006) Crystal structure of human D-amino acid oxidase: context-dependent variability of the backbone conformation of the VAAGL hydrophobic stretch located at the *si*-face of the flavin ring. *Protein Sci*. **15**, 2708–2717
21. Molla, G., Sacchi, S., Bernasconi, M., Pilone, M.S., Fukui, K., and Pollegioni, L. (2006) Characterization of human D-amino acid oxidase. *FEBS Lett*. **580**, 2358–2364

22. Todone, F., Vanoni, M.A., Mozzarelli, A., Bolognesi, M., Coda, A., Curti, B., and Mattevi, A. (1997) Active site plasticity in D-amino acid oxidase: a crystallographic analysis. *Biochemistry* **36**, 5853–5860

23. Pollegioni, L., Fukui, K., and Massey, V. (1994) Studies on the kinetic mechanism of pig kidney D-amino acid oxidase by site-directed mutagenesis of Tyrosine 224 and Tyrosine 228. *J. Biol. Chem*. **269**, 31666–31673

24. Katane, M., Osaka, N., Matsuda, S., Maeda, K., Kawata, T., Saitoh, Y., Sekine, M., Furuchi, T., Doi, I., Hirono, S., and Homma, H. (2013) Identification of novel D-amino acid oxidase inhibitors by in silico screening and their functional characterization in vitro. *J. Med. Chem.* **56**, 1894–1907

25. Subramanian, K., Góra, A., Spruijt, R., Mitusińska, K., Suarez-Diez, M., Martins dos Santos, V., and Schaap, P.J. (2018) Modulating D-amino acid oxidase (DAAO) substrate specificity through facilitated solvent access. *PLoS One* **13**, e0198990

26. Setoyama, C., Nishina, Y., Mizutani, H., Miyahara, I., Hirotsu, K., Kamiya, N., Shiga, K., and Miura, R. (2006) Engineering the substrate specificity of porcine kidney D-amino acid oxidase by mutagenesis of the "active-site lid". *J. Biochem*. **139**, 873–879

27. Miyano, M., Fukui, K., Watanabe, F., Takahashi, S., Tada, M., Kanashiro, M., and Miyake, Y. (1991) Studies on Phe-228 and Leu-307 recombinant mutants of porcine kidney D-amino acid oxidase: expression, purification, and characterization. *J. Biochem*. **109**, 171–177

28. Iwana, S., Kawazoe, T., Park, H.K., Tsuchiya, K., Ono, K., Yorita, K., Sakai, T., Kusumi, T., and Fukui, K. (2008) Chlorpromazine oligomer is a potentially active substance that inhibits human D-amino acid oxidase, product of a susceptibility gene for schizophrenia. *J. Enzyme Inhib. Med. Chem.* **23**, 901–911

29. Abou El-Magd, R.M., Sasaki, C., Kawazoe, T., El-Sayed, S.M., Yorita, K., Shishido, Y., Sakai, T., Nakamura, Y., and Fukui, K. (2010) Bioprocess development of the production

of the mutant P-219-L human D-amino acid oxidase for high soluble fraction expression in recombinant *Escherichia coli*. *Biochem. Eng. J*. **52**, 236–247

30. Setoyama, C., Miura, R., Nishina, Y., Shiga, K., Mizutani, H., Miyahara, I., and Hirotsu, K. (1996) Crystallization of expressed porcine kidney D-amino acid oxidase and preliminary X-ray crystallographic characterization. *J. Biochem*. **119**, 1114–1117
31. Massey, V. and Curti, B. (1966) A new method of preparation of D-amino acid oxidase apoprotein and a conformational change after its combination with flavin adenine dinucleotide. *J. Biol. Chem.* **241**, 3417–3423
32. Raibekas, A.A., Fukui, K., and Massey, V. (2000) Design and properties of human D-amino acid oxidase with covalently attached flavin. *Proc. Natl. Acad. Sci. U.S.A*. **97**, 3089–3093
33. Fonda, M.L. and Anderson, B.M. (1968) D-Amino acid oxidase: studies of flavin adenine dinucleotide binding. *J. Biol. Chem*. **243**, 5635–5643
34. Battye, T.G.G., Kontogiannis, L., Johnson, O., Powell, H.R., and Leslie, A.G.W. (2011) iMOSFLM: a new graphical interface for diffraction-image processing with MOSFLM. *Acta Crystallogr. D Biol. Crystallogr*. **67**, 271–281
35. Kabsch, W. (2010) XDS. *Acta Crystallogr. D Biol. Crystallogr*. **66,** 125–132
36. Vagin, A. and Teplyakov, A. (1997) MOLREP: an automated program for molecular replacement. *J. Appl. Cryst*. **30**, 1022–1025
37. Emsley, P., Lohkamp, B., Scott, W.G., and Cowtan, K. (2010) Features and development of Coot. *Acta Crystallogr. D Biol. Crystallogr*. **66**, 486–501
38. Adams, P.D., Afonine, P.V., Bunkóczi, G., Chen, V.B., Davis, I.W., Echols, N., Headd, J.J., Hung, L.W., Kapral, G.J., Grosse-Kunstleve, R.W., McCoy, A.J., Moriarty, N.W., Oeffner, R., Read, R.J., Richardson, D.C., Richardson, J.S., Terwilliger, T.C., and Zwart, P.H. (2010) PHENIX: a comprehensive Python-based system for macromolecular structure solution. *Acta Crystallogr. D Biol. Crystallogr*. **66**, 213–221

39. Kato, Y., Hin, N., Maita, N., Thomas, A.G., Kurosawa, S., Rojas, C., Yorita, K., Slusher, B.S., Fukui, K., and Tsukamoto, T. (2018) Structural basis for potent inhibition of D-amino acid oxidase by thiophene carboxylic acids. *Eur. J. Med. Chem*. **159**, 23–34

40. Lovell, S.C., Davis, I.W., Adrendall, W.B.III, de Bakker, P.I.W., Word, J.M., Prisant, M.G., Richardson, J.S., and Richardson, D.C. (2003) Structure validation by Cα geometry: Φ, Ψ and Cβ deviation. *Proteins* **50**, 437–450

41. Guex, N. and Peitsch, M.C. (1997) SWISS-MODEL and the Swiss-PdbViewer: an environment for comparative protein modeling. *Electrophoresis* **18**, 2714–2723

42. Molla, G. (2017) Competitive inhibitors unveil structure/function relationships in human D-amino acid oxidase. *Front. Mol. Biosci*. **4**, 1–17

43. Kawazoe, T., Tsuge, H., Imagawa, T., Aki, K., Kuramitsu, S., and Fukui, K. (2007) Structural basis of D-DOPA oxidation by D-amino acid oxidase: alternative pathway for dopamine biosynthesis. *Biochem. Biophys. Res. Commun*. **355**, 385–391

44. Yoshimatsu, H., Yonezawa, A., Yamanishi, K., Yao, Y., Sugano, K., Nakagawa, S., Imai, S., Omura, T., Nakagawa, T., Yano, I., Masuda, S., Inui, K.I., and Matsubara, K. (2016) Disruption of *Slc52a3* gene causes neonatal lethality with riboflavin deficiency in mice. *Sci. Rep*. **6**, 27557

45. Abou El-Magd, R.M., Park, H.K., Kawazoe, T., Iwana, S., Ono, K., Chung, S.P., Miyano, M., Yorita, K., Sakai, T., and Fukui, K. (2010) The effect of risperidone on D-amino acid oxidase activity as a hypothesis for a novel mechanism of action in the treatment of schizophrenia. *J. Psychopharmacol*. **24**, 1055–1067

46. Terry-Lorenzo, R.T., Chun, L.E., Brown, S.P., Heffernan, M.L.R., Fang, Q.K., Orsini, M.A., Pollegioni, L., Hardy, L.W., Spear, K.L., and Large, T.H. (2014) Novel human D-amino acid oxidase inhibitors stabilize an active-site lid-open conformation. *Biosci. Rep*. **34**, 487–499

47. Nelson, D.L., and Cox, M.M. (2004) *Lehninger Principles of Biochemistry*, 4th edition, pp. 78–80, W.H. Freeman, New York

48. Hondo, T., Warizaya, M., Niimi, T., Namatame, I., Yamaguchi, T., Nakanishi, K., Hamajima, T., Harada, K., Sakashita, H., Matsumoto, Y., Orita, M., and Takeuchi, M. (2013) 4-Hydroxypyridazin-3(2*H*)-one derivatives as novel D-amino acid oxidase inhibitors. *J. Med. Chem*. **56**, 3582–3592

49. Mattevi, A., Vanoni, M.A., Todone, F., Rizzi, M., Teplyakov, A., Coda, A., Bolognesi, M., and Curti, B. (1996) Crystal structure of D-amino acid oxidase: a case of active site mirror-image convergent evolution with flavocytochrome b_2. *Proc. Natl. Acad. Sci. U.S.A.* **93**, 7496–7501

50. Mizutani, H., Miyahara, I., Hirotsu, K., Nishina, Y., Shiga, K., Setoyama, C., and Miura, R. (1996) Three-dimensional structure of porcine kidney D-amino acid oxidase at 3.0 Å resolution. *J. Biochem*. **120**, 14–17

51. Sinnokrot, M.O., Valeev, E.F., and Sherrill, C.D. (2002) Estimates of the ab initio limit for π-π interactions: the benzene dimer. *J. Am. Chem. Soc*. **124**, 10887–10893

52. Hallberg, B.M., Leitner, C., Haltrich, D., and Divne, C. (2004) Crystal structure of the 270 kDa homotetrameric lignin-degrading enzyme pyranose 2-oxidase. *J. Mol. Biol.* **341**, 781–796

53. Denessiouk, K.A., Rantanen, V.V., and Johnson, M.S. (2001) Adenine recognition: a motif present in ATP-, CoA-, NAD-, NADP-, and FAD-dependent proteins. *Proteins* **44**, 282–291

54. Chakrabarti, P. and Samanta, U. (1995) CH/π interaction in the packing of the adenine ring in protein structures. *J. Mol. Biol*. **251**, 9–14

55. Pettersen, E.F., Goddard, T.D., Huang, C.C., Couch, G.S., Greenblatt, D.M., Meng, E.C., and Ferrin, T.E. (2004) UCSF Chimera-a visualization system for exploratory research and analysis. *J. Comput. Chem.* **25**, 1605–1612

Figure legends

Fig. 1 Apparent kinetic parameters of holo-human DAO with a high concentration of FAD. The kinetic parameters of holo wild-type and P219L DAOs were determined with a saturated FAD concentration (final conc. ~20 μM) and are displayed as the (A) k_{cat}, (B) K_m, and (C) k_{cat}/K_m values. Data are presented as the mean ± SD (n = 3 for wild-type and n = 4 for P219L). *$p < 0.05$, ***$p < 0.001$ (Student's *t*-test) in comparison to control (wild-type human DAO).

Fig. 2 Apparent kinetic parameters of FAD-reconstituted human DAO with a low concentration of FAD. The kinetic parameters of reconstituted wild-type and P219L DAOs were determined with a low concentration of FAD (final conc. ~2 μM) and are displayed as the (A) k_{cat}, (B) K_m, and (C) k_{cat}/K_m values. Data are presented as the mean ± SD (n = 3 for wild-type and n = 4 for P219L). *$p < 0.05$, **$p < 0.01$, ***$p < 0.001$ (student's t-test), compared with control (wild-type human DAO).

Fig. 3 The inhibition constant (K_i) of benzoate for wild-type and P219L DAOs. The K_i values are presented as the mean ± SD (n =3 for wild-type and n = 4 for P219L). *$p < 0.05$, ***$p < 0.001$ (Student's *t*-test) in comparison to control (wild-type human DAO).

Fig. 4 Distances between atoms around the active site and the lid of P219L and wild-type DAOs. (A) Atomic distances in the active site of human DAO complexed with benzoate and FAD. The distances were calculated by Swiss-PdbViewer (*41*) and are presented as the mean ± SD of 4 molecules within the asymmetric unit. The distances between atoms forming H-bonds ((1) - (3)) are displayed as dashed green lines, whereas those between the atoms of benzoate and FAD ((4), (5)) are displayed as black arrows. The orange arrows indicate possible π-π interactions. (B) Atomic distances between H-bond-forming atoms in the active site lid of human DAO. The superimposed structures of the active site lids (residue 216-228) of P219L and wild-type are shown as green and orange lines, respectively. The dashed green lines indicate the atomic distances in the active site lid between (1) Asp218 (C=O) - Arg221 (NH), (2) Asp218 (C=O) - Gly222 (NH), (3) Gly222 (C=O) - Asn225 (NH), and (4) Pro227 (C=O) - Thr216 (NH).

Fig. 5 The structural change of Tyr224 and benzoate in the P219L complex. (A) Top views of Tyr224 and benzoate in the ternary complexes. The left panel shows the superimposed structures of the wild-type (PDB ID: 2DU8) and P219L complexes, whereas the middle and right panels separately show the structures of the wild-type and P219L complexes, respectively. The line model of Tyr224 of P219L is colored in green, whereas the other line models are colored in CPK. The yellow arrows indicate the directions of the movement of Tyr224 and benzoate in the P219L complex with respect to those in the wild-type complex. The dotted black lines between the aromatic rings of Tyr224 and benzoate indicate mean atomic distances of 4 DAO molecules within the asymmetric unit. (B) Side views of the individual panels of (A).

Fig. 6 Acetic acid in the ternary complex of P219L. (A) Cross section of a monomer of P219L with surface charge distribution. In the complex structure, FAD and benzoate were located within the internal cavity, whereas the acetic acid molecule was located at one of the entrance/exit pathways of the cavity. (B) The sphere model of the acetic acid molecule surrounded by several amino acid residues around the adenine ring pocket. Atoms other than carbons are colored in CPK, whereas the carbons of P219L residues, FAD and acetic acid are colored in gray, pale cyan, and pale green, respectively. The H-bond between acetic acid and water is represented as a yellow line.

Supplementary Data

Supplementary Data are available at *JB* Online.

Funding

This work was supported in part by Japan Science and Technology Agency; CREST (Core Research for Evolutionary Science and Technology); a grant for Enzyme Research from the Japan Foundation for Applied Enzymology; and JSPS KAKENHI (Grant Number 18K06580). An Udon Thani Rajabhat University Scholarship was awarded to W.R.

Acknowledgements

We thank Tomoya Kawazoe for providing the characteristic features of human and porcine DAOs. We also acknowledge Hiroyuki Sumitomo for preliminary results of the kinetic parameters of wild-type and P219L human DAOs. We thank the beamline staff at the Photon Factory (proposal No: 2017G615 and 2019G050) for supporting the data collection.

Conflict of Interest

None declared.

Fig. 1

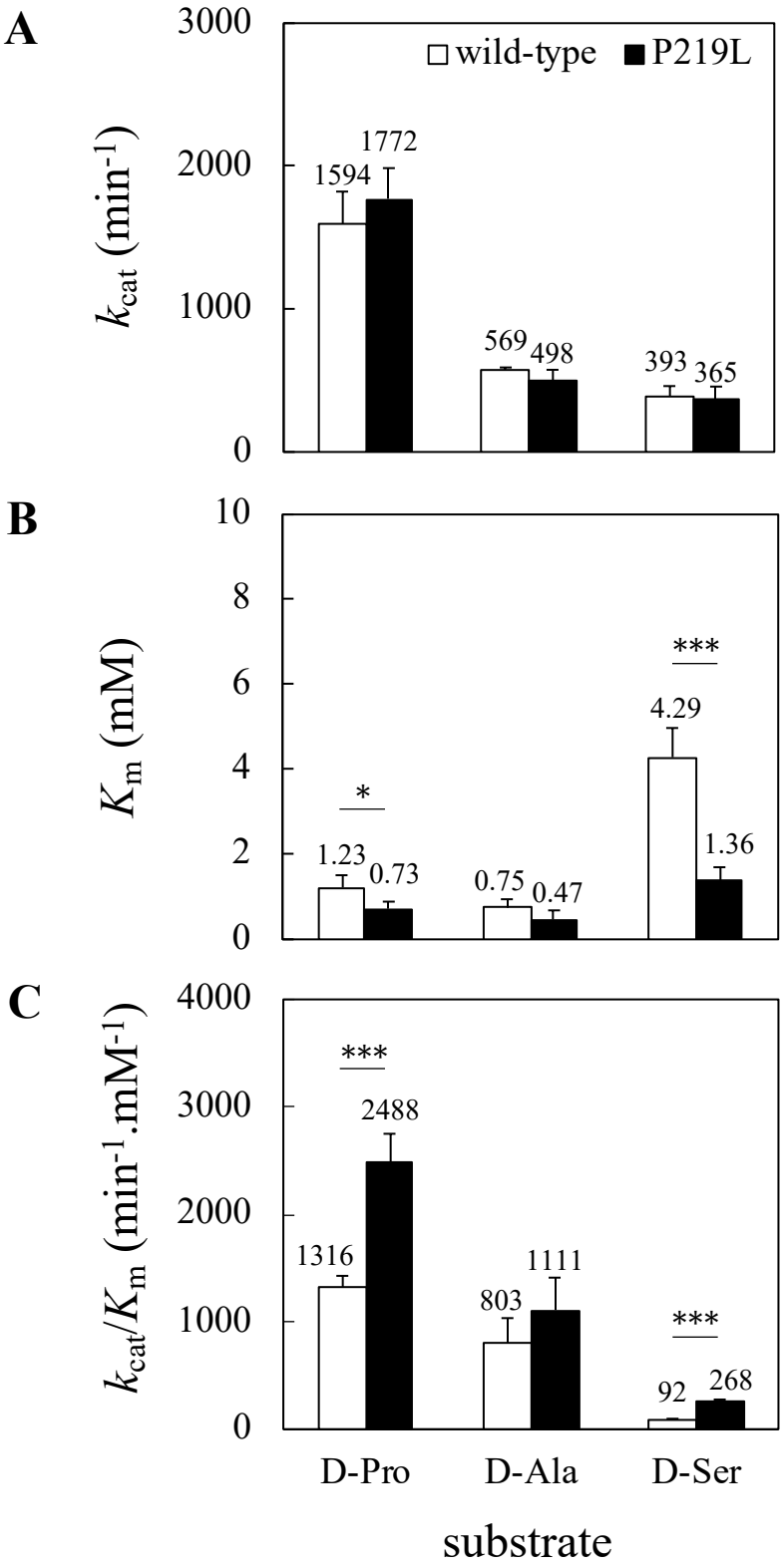

Fig. 2

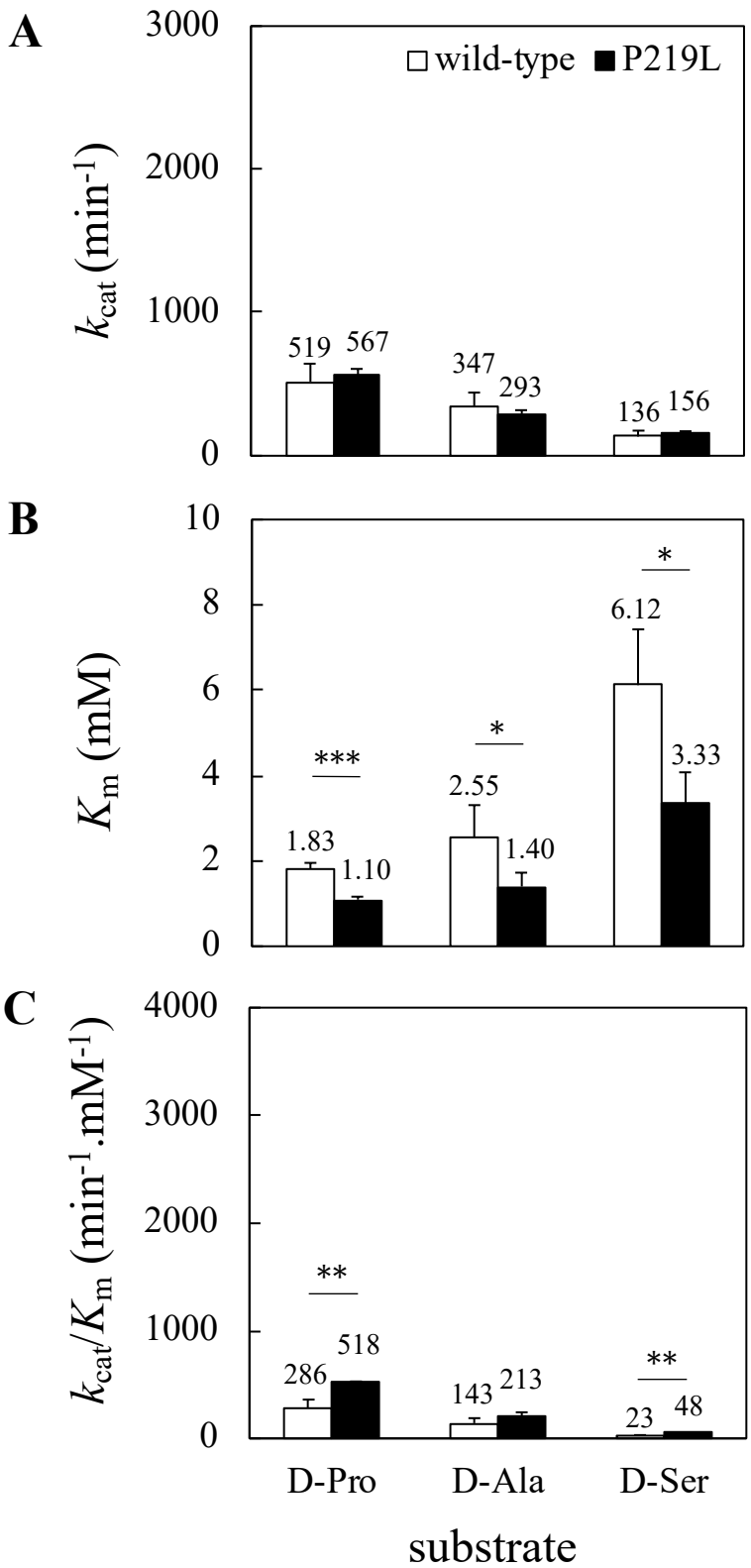

Fig. 3

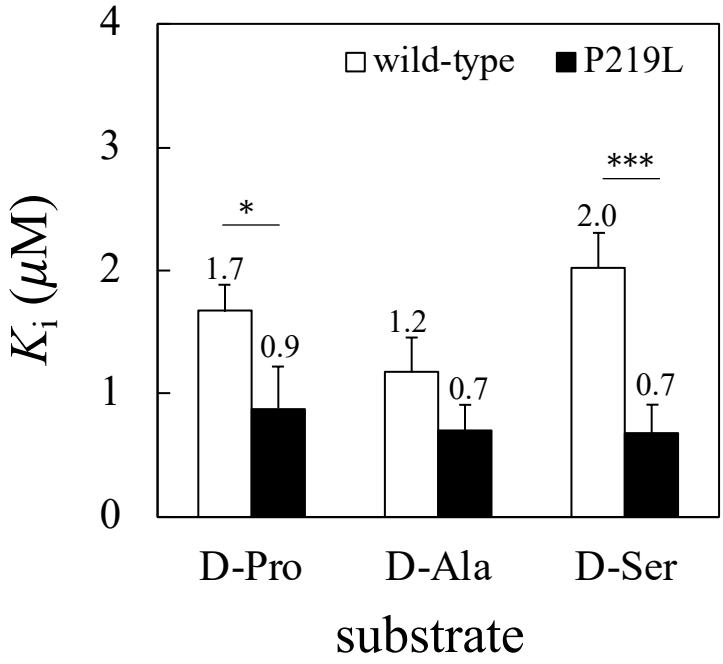

Fig. 4

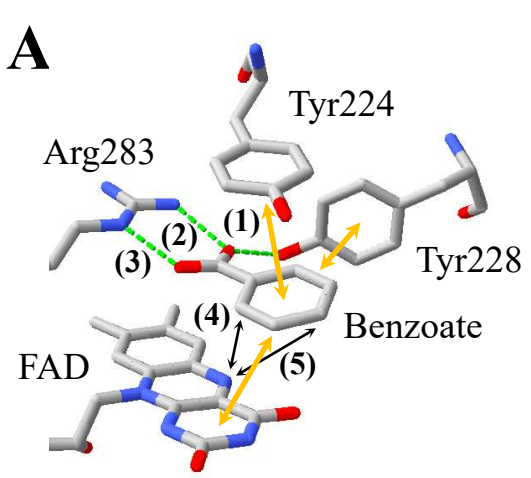

	P219L	wild-type
(1)	2.66 ± 0.02	2.83 ± 0.16
(2)	2.75 ± 0.12	2.90 ± 0.13
(3)	2.71 ± 0.06	3.01 ± 0.08
(4)	3.52 ± 0.10	3.62 ± 0.04
(5)	4.80 ± 0.07	5.10 ± 0.08

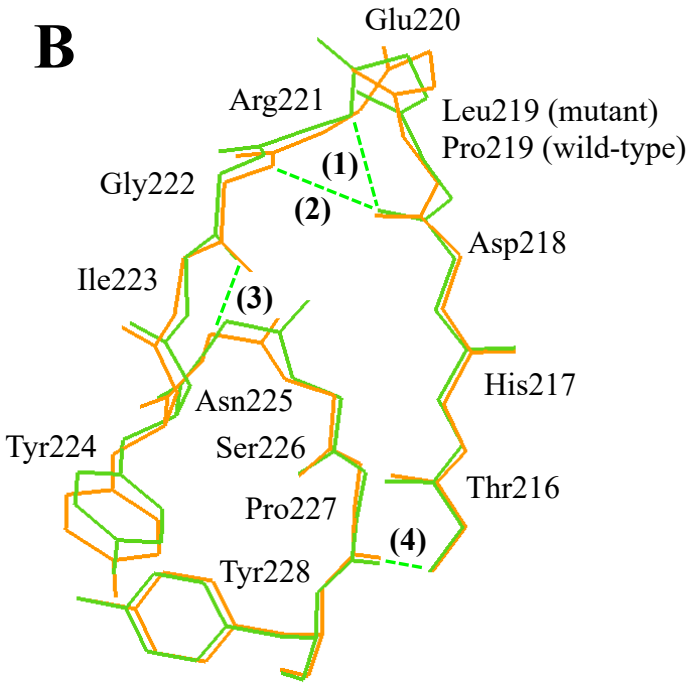

	P219L (Green)	wild-type (Orange)
(1)	3.08 ± 0.09	3.31 ± 0.13
(2)	3.41 ± 0.17	3.14 ± 0.13
(3)	3.24 ± 0.10	3.24 ± 0.15
(4)	3.07 ± 0.02	3.17 ± 0.08

Fig. 5

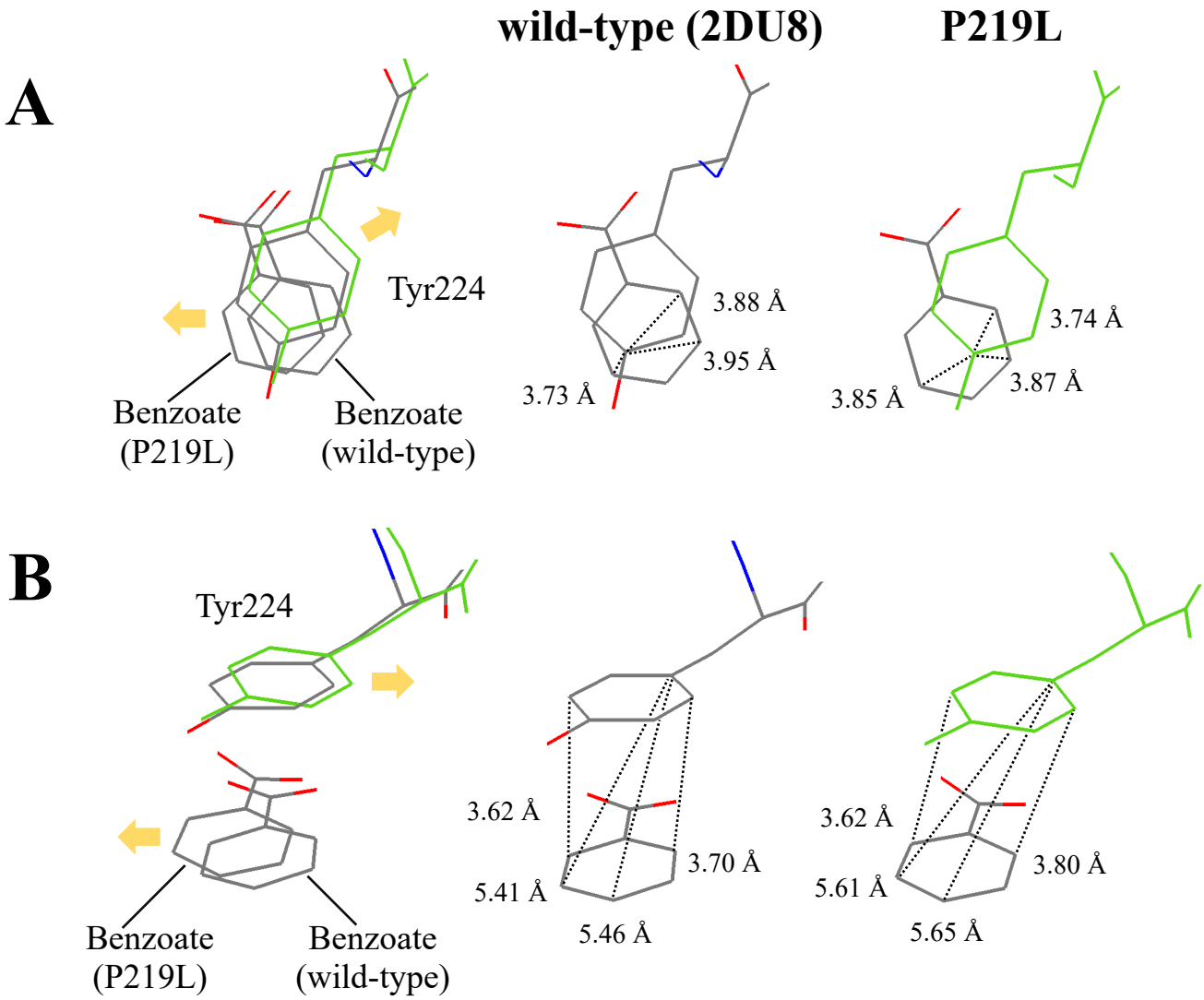

Fig. 6

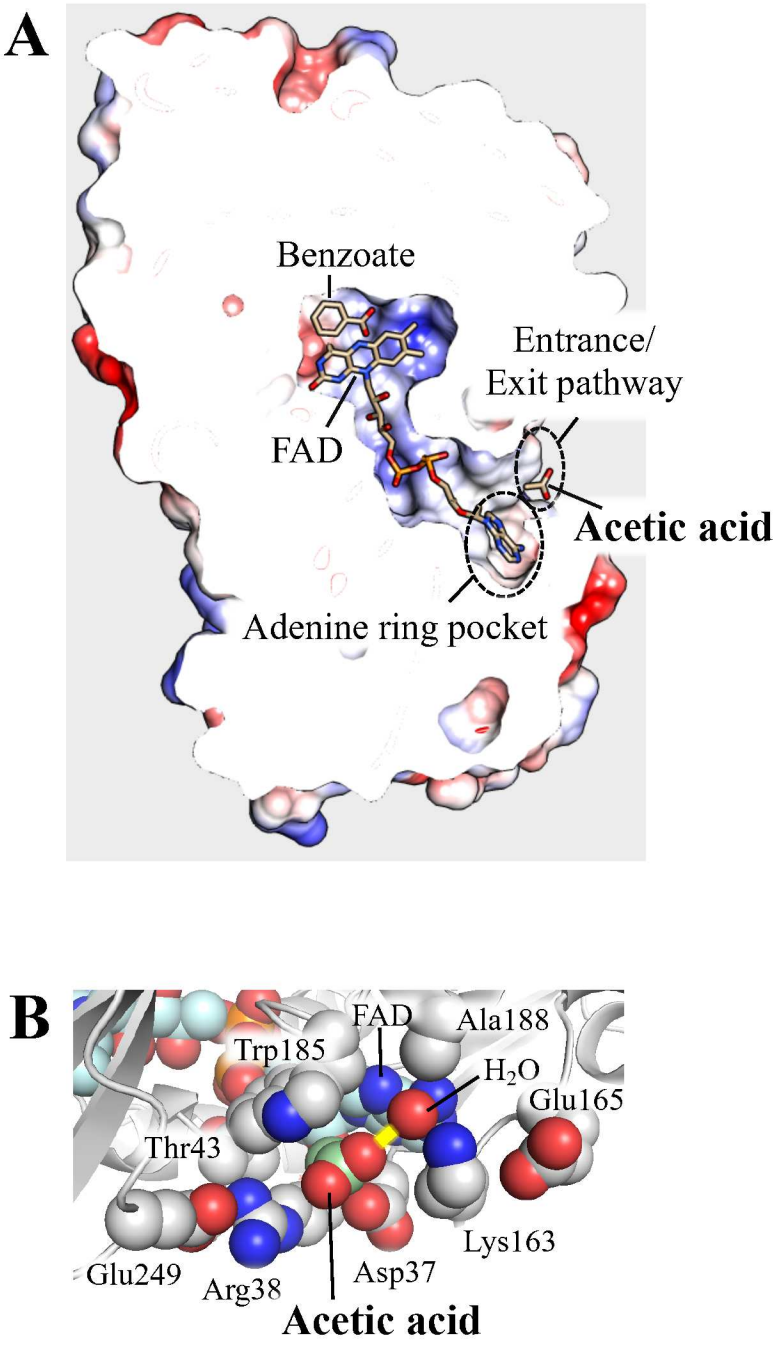

Table I. Data collection statistics.

Data collection	
X-ray source	Photon Factory BL5A
Wavelength (Å)	1.000
Space group	$P2_12_12$
Unit cell a, b, c (Å)	149.49, 182.78, 51.04
Resolution (Å)	48.30 – 2.25 (2.30 – 2.25)
Unique reflections	67,535 (4,496)
R_{meas}	0.066 (1.002)
I/σI	21.3 (2.2)
Completeness (%)	99.9 (100.0)
Redundancy	6.6 (6.4)
half-data set correlation (CC (1/2))	1.00 (0.81)

[a] Highest resolution shell is shown in parentheses.

Table II. Refinement statistics.

Refinement	P219L
Resolution (Å)	48.3 – 2.25 (2.28 – 2.25) [b]
No. reflections	67,432
R_{work}/R_{free}	0.1887/0.2485
RMSD	
Bond lengths (Å)	0.009
Bond angles (°)	1.163
No. atoms	
Protein	10,833
FAD	212
Benzoate	36
Acetic acid	8
Water	390
Average B-factors (Å^2)	
Overall	46.77
Protein	47.01
FAD	37.95
Benzoate	39.30
Acetic acid	57.48
Water	45.44
Ramachandran plot [a]	
Favored region	95.8%
Allowed region	4.2%
Outlier region	0.0%
PDB code	6KBP

[a] Analyzed by RAMPAGE (*40*).

[b] The highest resolution shell is shown in parentheses.